Polym. Bull. (2014) 71:2981–2997
DOI 10.1007/s00289-014-1236-9

ORIGINAL PAPER

Effect of nano-ZnO-supported 13X zeolite on photo-oxidation degradation and antimicrobial properties of polypropylene random copolymer

Mei Li · Gu Li · Yifei Fan · Juan Jiang · Qian Ding · Xin Dai · Kancheng Mai

Received: 12 February 2014 / Revised: 18 August 2014 / Accepted: 23 August 2014 /
Published online: 14 September 2014

Abstract To improve the photo-oxidation degradation resistance and antimicrobial ability of ZnO-filled polypropylene random copolymer (PPR), 13X zeolite particles supported with nano-ZnO with different morphologies were prepared and used to manufacture filled PPR composites. The formation of ZnO with different morphologies on the surface of 13X zeolite was proved by atomic absorption spectroscopy, scanning electron microscope, UV–vis spectra, and fluorescence spectra. The results indicated that the photo-oxidation degradation resistance of nano-ZnO-supported 13X zeolite-filled PPR composites is higher than that of PPR composites filled by the same content of pure nano-ZnO. Antimicrobial experiment results show that nano-ZnO-supported 13X zeolite-filled PPR composites exhibit higher antimicrobial properties than ZnO-filled PPR composites prepared by directly adding nano-ZnO into PPR matrix for *Staphylococcus aureus* and *Escherichia coli*. The addition of nano-ZnO-supported 13X zeolite particles increases the crystallization temperature, but has no influence on the melting behavior of PPR composites.

Keywords Polypropylene random copolymer (PPR) · ZnO · Photo-oxidation degradation · Antimicrobial properties

M. Li · G. Li (✉) · Y. Fan · J. Jiang · Q. Ding · X. Dai · K. Mai (✉)
Materials Science Institute, School of Chemistry and Chemical Engineering, Sun Yat-sen University, Guangzhou 510275, People's Republic of China
e-mail: ceslg@mail.sysu.edu.cn

K. Mai
e-mail: cesmkc@mail.sysu.edu.cn

M. Li · G. Li · Y. Fan · J. Jiang · Q. Ding · X. Dai · K. Mai
Key Laboratory of Polymeric Composites and Functional Materials of Ministry of Education, Key Laboratory of High Performance Polymer-based Composites of Guangdong Province, Guangzhou 510275, People's Republic of China

Introduction

Polypropylene random copolymer (PPR) is a kind of thermoplastic material developed in recent years. PPR copolymerized by propylene and ethylene has been widely used for pipes, automobiles parts, furniture and packing plastic because of its excellent physical and mechanical properties [1–4]. At present, the crystalline structure, morphology, and mechanical and rheological properties of PPR have been reported [5–7]. PPR, similar to iPP homopolymer materials, easily undergoes photo-oxidation degradation. However, the photo-oxidation degradation characteristic of PPR composites has little been investigated. In addition, it is needed to increase the antimicrobial properties of PPR, which is used as pipes and packing plastic. As is known, the addition of nano particles is an effective method to offer functionality and improve the physical and mechanical properties of polymer materials.

Nano-ZnO is a kind of inorganic particle with antibacterial ability, acts as UV light screen and has catalytic and electrical properties [8–14]. The addition of nano-ZnO generally improves the antibacterial ability and reduces the photo-oxidation degradation of polymer materials. The photo-oxidation degradation resistance and antibacterial ability of nano-ZnO-filled PP composites have been investigated [15–17]. Zhao et al. [15] investigated the photo-oxidation degradation of nano-ZnO-filled PP composites and observed that photo-oxidation degradation can be reduced significantly due to the superior UV light screen effect offered by nano-ZnO particles. Chandramouleeswaran et al. [16] observed that nano-ZnO not only reduced the photo-oxidation degradation, but also improved the antibacterial ability of PP against two human pathogenic bacteria, *Staphylococcus aureus* and *Escherichia coli*. Many investigations found that the particle size, morphology, and physical and chemical properties of ZnO varied with the preparation methods [16, 18–22]. Venkatesha et al. [18] used the electrochemical method to synthesize flower-shaped ZnO with good photo-catalytic properties. Hassana et al. [19] fabricated one-dimensional ZnO nanostructures through thermal evaporation via the vapor solid mechanism on different substrates. The crystallization behavior and mechanical properties of PP composites filled by nano-ZnO with different morphologies have been investigated [23–26]. To develop PP films for food-packing applications, Lepot et al. [24] prepared biaxial orientation PP films containing spherical and nanorod nano-ZnO particles and found that nanorod ZnO-filled PP films exhibited better mechanical properties. Omar et al. [25] studied the physical and mechanical properties of PP composites filled by nano-ZnO with different morphologies and observed that addition of 1 wt% nano-ZnO improved the tensile strength, tensile modulus and elongation at the break of PP and nanorod ZnO-filled PP exhibited better ultraviolet resistance. Zheng et al. [23] and Wen et al. [26] investigated the crystallization behavior and mechanical properties of PP composites filled by tetra-needle-shaped zinc oxide whisker (T-ZnO_w).

Although nano-ZnO-filled PP composite has been widely investigated [15–17, 27], ZnO-filled PPR composites are little reported, especially PPR composites filled by nano-ZnO supported on surface of inorganic particles [28]. In this paper, nano-ZnO-supported 13X zeolites with different morphologies were prepared using 13X zeolite as support and their filled PPR composites were fabricated. The photo-

oxidation degradation characteristic, antimicrobial ability and crystallization properties of PPR composites filled by nano-ZnO-supported 13X zeolite were investigated and compared with PPR composites directly filled by the same content of nano-ZnO. A new method was developed to prepare PPR composites with improved photo-oxidation degradation resistance and antimicrobial ability.

Experimental

Materials

PPR (R200P, MRI = 0.23 g/10 min at 23 °C and 2.16 kg, the content of ethylene is 3.8 %, Mn = 72.2×10^4 g/mol, Mw/Mn = 4.5 and the density is 0.91 g/cm^3) was provided by Hyosung Corporation. 13X zeolite with average particle size of about 1.0 μm and pore diameter about 1.0 nm was supplied by Wuxi Rongdeli Molecular Sieve Factory, China. $Zn(Ac)_2$ (AR) was supplied by Tianjin Miou Chemistry Co. Ltd, China. $Zn(NO_3)_2$ (AR), NaOH (AR) and concentrated nitric acid (GR) were bought from Guangzhou Chemical Factory, China. *E. coli* and *S. aureus* with the concentration of 1.7×10^7 CFU/ml and 5.5×10^6 CFU/ml, respectively, were obtained from Guangzhou Institute of Microbiology, China. Nano-ZnO with average particle size of about 30 ± 10 nm was supplied by Aladdin Chemistry Co. Ltd.

Preparation of materials

Preparation of nano-ZnO-supported 13X zeolite particles

Neat 13X zeolite was pretreated at 400 °C in a muffle furnace for 3 h; then 20 g of pretreated zeolite was added into a three-neck flask. After the system was evacuated to 0.063 MPa with a vacuum pump and keeping the pressure for 0.5 h to remove the air in the flask and the hole of zeolite, 120 ml of aqueous solution with different concentrations of zinc acetate and zinc nitrate was added into the three-neck flask and the mixture stirred for 2 h. Then the filtered mixture was transferred to a beaker after vacuum filtering. 1 mol/l NaOH was added to adjust the pH of the mixture at 7.0, and then the mixture stirred for 1 h. The filtered mixture was heated from room temperature to 300 °C in a muffle furnace to obtain nano-ZnO-supported 13X zeolite. The nanno-ZnO-supported 13X zeolite particles prepared with concentrations of 1, 3, 5, 7 and 10 wt% zinc acetate and zinc nitrate aqueous solution were, respectively, denoted as A_1, A_3, A_5, A_7, A_{10} and N_1, N_3, N_5, N_7, N_{10}. The content of ZnO in the nano-ZnO-supported 13X zeolite was measured by atomic absorption spectroscopy (AAS).

Preparation of nano-ZnO-supported 13X zeolite-filled PPR composites

PPR composites were prepared with an HL-200 internal mixer (Jilin University Science and Education Instrument Factory, China) at 170 °C and 50 rpm for 7 min. The nano-ZnO-supported 13X zeolite-filled PPR composites prepared with 5, 10, 15

and 20 phr A_{10} or N_{10} were denoted as $5A_{10}$/PPR, $10A_{10}$/PPR, $15A_{10}$/PPR, $20A_{10}$/PPR and $5N_{10}$/PPR, $10N_{10}$/PPR, $15N_{10}$/PPR, $20N_{10}$/PPR. The ZnO/PPR composites containing the same ZnO content as that of $5N_{10}$/PPR, $10N_{10}$/PPR, $15N_{10}$/PPR and $20N_{10}$/PPR were denoted as ZnO_5/PPR, ZnO_{10}/PPR, ZnO_{15}/PPR and ZnO_{20}/PPR. 10 phr pure 13X zeolite-filled PPR composites were denoted as 10S/PPR. The neat PPR and filled PPR composite films for photo-oxidation degradation and antimicrobial experiments were pressed on XLB 50-D plate vulcanizing press (Zhejiang Shuangli Group Huzhou Xingli Rubber Machinery Manufacturing Company, China) at 180 °C and 10 MPa for 3 min and then quickly cooled to room temperature. The morphology of nano-ZnO-supported 13X zeolite dispersed in PPR was invested with mold samples. The samples were prepared by an F-120 vertical injection molding machine (Guangzhou Fengtie Mechanical Company, China) at a temperature of 230 °C, injection pressure of 60 MPa and mold temperature of 60 °C.

Characterization

Zinc oxide contents

Nano-ZnO-supported 13X zeolite of 5 mg was dissolved in concentrated nitric acid and diluted by deionized water. The ZnO contents in nano-ZnO-supported 13X zeolite were characterized on Japan Hitachi Z-2000 atomic absorption spectroscopy (AAS), The analytical line of Zn is 213.9 nm, The content of ZnO is obtained with the following formula:

$$W_{\mathrm{ZnO}}\ \% \ = \frac{C_{\mathrm{Zn}} \times V \times M_{\mathrm{ZnO}}}{M_{\mathrm{Zn}} \times m_{\mathrm{s}}} \times 100\ \%\ , \tag{1}$$

in which W_{ZnO} is the mass content of ZnO in nano-ZnO-supported 13X zeolite; C_{Zn} (ppm), V(L) and m_{s} (g) are the concentration, volume and mass of the sample, respectively. M_{ZnO} and M_{Zn} are the molar mass of ZnO and Zn, respectively.

Zeolite morphology

The morphology of 13X zeolite, nano-ZnO-supported 13X zeolite and nano-ZnO particles was observed with a scanning electron microscope (SEM S4800, Hitachi, Japan). The injection molding samples were fractured in liquid nitrogen, and the morphology of filled PPR composites and dispersion of zeolite in PPR were obtained. The samples were gold coated and observed under an acceleration voltage of 20 kV and a current of 20 μA.

UV–vis spectra

The UV–vis spectra of 13X zeolite and nano-ZnO-supported 13X zeolite particles were measured on a UV-3150 (Shimadzu, Japan), at slit width of 5 nm and scanning number of 200–600 nm. $BaSO_4$ was used as the reference sample.

Fluorescence spectra

The fluorescence spectra of 13X zeolite, ZnO and nano-ZnO-supported 13X zeolite particles were characterized by fluorescence spectroscopy (RF-5301PC, Shimadzu, Japan), at an excitation wavelength of 320 nm and emission wavelength of 330–800 nm. The slit width of excitation and emission is 10 nm and the optical filters of incident light and emitted light are 250–400 and 360 nm, respectively.

Photo-oxidation degradation

Photo-oxidation degradation for PPR composites films (the thick is about 20 μm) was carried out under a UV lamp with power of 125 W (the UV-irradiation wavelength was 300–400 nm). The temperature of the sample surface was 80 °C and the vertical irradiation distance 20 cm. Composite films subjected to UV irradiation for 0, 50, 90 and 120 h, respectively, were characterized by FTIR analysis. The FTIR measurement (model Nicolet Nexus 670) was carried out with the scanning range of 4,000–500 cm^{-1} and resolution ratio 4 cm^{-1}, at transmission mode using 32 scans. The carbonyl index, characterizing the degree of photo-oxidation degradation of PPR composites, was calculated by the Eq. 2 [29]:

$$\text{Carbonyl index} = \frac{A_R}{A_C}. \tag{2}$$

In Eq. 2, A_C is the area of the carbonyl adsorption band between 1,700 and 1,800 cm^{-1} and A_R is the area of the reference band between 2,700 and 2,750 cm^{-1}. The reference band was not affected by photo-oxidation degradation or crystallization degree of PPR [30].

Antibacterial property

The antimicrobial ability of nano-ZnO-supported 13X zeolite-filled PPR composites was evaluated quantitatively in fluid nutrient medium [31, 32]. The films of composites at 1 g with the dimensions of 1 cm length × 1 cm width × 0.12 cm thickness were soaked in the 2 ml fluid nutrient medium after sterilization at 37 °C for 18 h in a shaker and the intensity of UV absorption, A value, of the nutrient solution was measured by UV–vis spectrophotometer (TU-1901, Beijing Purkinje General Instrument Co. Ltd. China). The antibacterial reduction rate, Y value, was obtained with the following formula [33]:

$$Y\,\% = [(A_b - A_s)/A_b] \times 100\,\%, \tag{3}$$

in which A_b and A_s are the intensity of UV absorption of blank and samples under the incident wavelength of 600 nm, respectively.

Crystallization and melting behavior

The crystallization behavior and melting characteristics of PPR and its composites were studied on a TA Q20 differential scanning calorimeter in a nitrogen atmosphere. About 5 mg of sample was heated to 220 °C at a rate of 30 °C/min and held at this temperature for 5 min to erase the thermal and mechanical history. Samples were cooled to 40 °C, held at this temperature for 3 min and then reheated to 220 °C at a rate of 10 °C/min. The crystallinity was determined by $X_c\ \% = (\Delta H/\Delta H_0) \times 100\ \%$, in which ΔH and ΔH_0 were the melting enthalpy of the samples and 100 % crystalline PP, respectively, and $\Delta H_0 = 209$ J/g [5].

Results and discussion

Morphology and characterization of nano-ZnO-supported 13X zeolite

The content of ZnO in nano-ZnO-supported 13X zeolite prepared with $Zn(Ac)_2$ and $Zn(NO_3)_2$ aqueous solution is listed in Table 1. It can be seen that the content of ZnO supported on the surface of 13X zeolite increased with increase in the zinc salt concentration. The ZnO of 15.2 % supported on 13X zeolite was obtained with the salt in which aqueous concentration was 10 %. To obtain better ultraviolet resistance and antimicrobial ability, nano-ZnO-supported 13X zeolite of A_{10} and N_{10} with high ZnO content was used to prepared PPR composites.

The SEM morphologies of 13X zeolite, nano-ZnO and nano-ZnO-supported 13X zeolite particles are shown in Fig. 1. It can be observed that the 13X zeolite has regular shape and smooth surface, while the surface of nano-ZnO-supported 13X zeolite is different from zeolite and has filamentous or granular shape, indicating the formation of ZnO supported on the surface of zeolite. In addition, the filamentous ZnO supported on the surface of zeolite with nanoscale was observed. Secondly, the size of filamentous ZnO supported on the surface of zeolite is lower than that of pure nano-ZnO particles. It indicated that the ZnO supported on the surface of zeolite has larger specific area than that of pure nano-ZnO. As a result, the nano-ZnO-supported 13X zeolite is expected to exhibit better ultraviolet resistance and antimicrobial ability. Moreover, the particle size of ZnO supported on N_{10} is smaller than the one supported on A_{10}, so the specific area of the former is larger than the latter. This is probably the reason that the photo-stability of N_{10}-filled PPR composites is better than A_{10}-filled PPR composites.

Table 1 Amount of ZnO in nano-ZnO-supported 13X zeolite prepared by different mass concentrations of zinc acetate or zinc nitrate

Zeolite	S	A_1	A_3	A_5	A_7	A_{10}
Content of ZnO (%)	0	2.1	7.0	10.8	11.8	15.2
Zeolite	–	N_1	N_3	N_5	N_7	N_{10}
Content of ZnO (%)	–	1.4	6.3	7.4	11.6	15.2

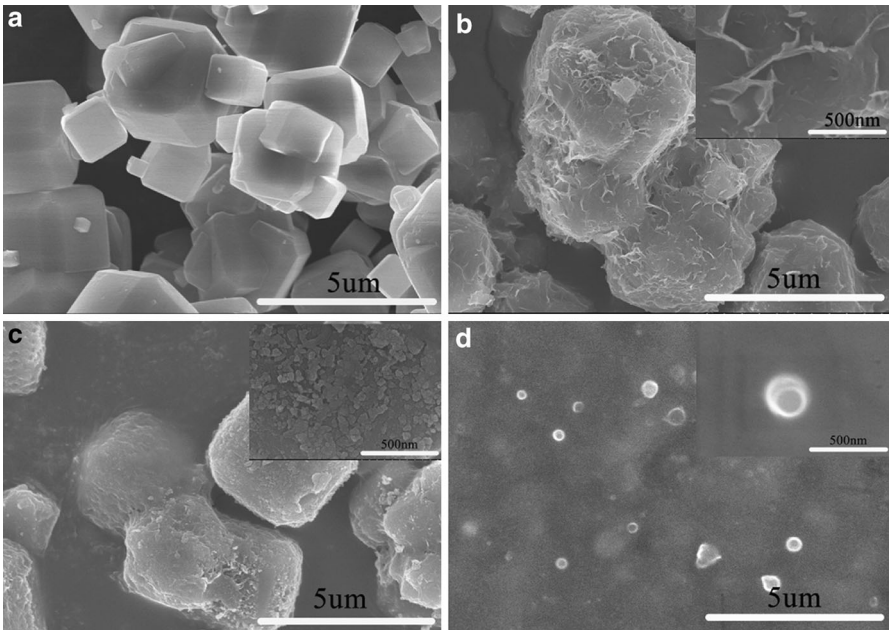

Fig. 1 SEM morphologies of zeolite (**a**), A_{10} (**b**), N_{10} (**c**) and nano-ZnO (**d**)

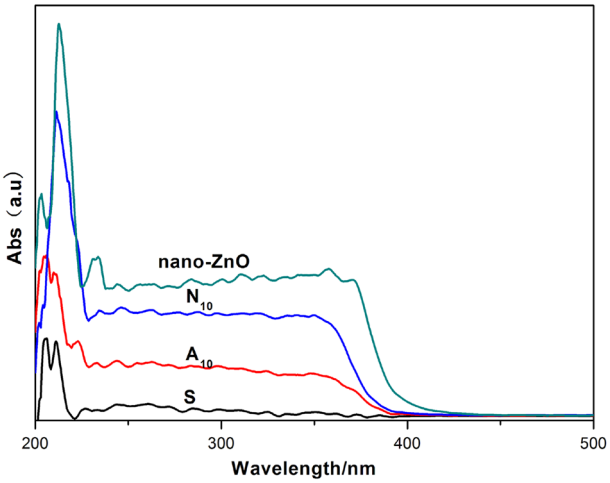

Fig. 2 UV–vis spectra of 13X zeolite (S), nano-ZnO-supported 13X zeolite (A_{10} and N_{10}) and nano-ZnO in the range of 200–500 nm

The UV–vis spectra of 13X zeolite, nano-ZnO and nano-ZnO-supported 13X zeolite particles are shown in Fig. 2. It can be observed that the intensity of UV absorption of pure ZnO is highest and 13X zeolite has no UV absorption in the

range of 200–400 nm. Nano-ZnO-supported 13X zeolite of A_{10} or N_{10} has UV absorption in the range of 200–400 nm, which also proved the formation of ZnO on the surface of 13X zeolite. The blue shift of UV absorption for ZnO supported on the surface of zeolite particles is attributed to the formation of smaller size of ZnO on the surface of zeolite [23]. Besides, the higher intensity of UV absorption of N_{10} than A_{10} should result in the better ultraviolet resistance of N_{10}-filled PPR composites. In addition, the intensity of UV absorption of N_{10} is higher than A_{10}, and it is expected to provide the basis for the result that the photo-stability of N_{10}-filled PPR composite is better than A_{10}-filled PPR composite.

Figure 3 presents the fluorescence spectra of 13X zeolite, nano-ZnO and nano-ZnO-supported 13X zeolite particles with slit width of excitation and emission of 5 nm at excitation wavelength of 320 nm. It can be seen that nano-ZnO has a fluorescence emission band at 550 nm, while no emission band is observed for 13X zeolite particles. The lower intensity of fluorescence emission band at 550 nm of ZnO than A_{10} or N_{10} is due to fluorescence quenching in the high content of ZnO. The strong intensity of fluorescence emission band at 550 nm of nano-ZnO-supported 13X zeolite particles indicated the formation of ZnO supported on the surface of zeolite. It can be seen from Fig. 1 that ZnO with different sizes and morphologies supported on the surface of zeolite resulted in different intensity of fluorescence emission of A_{10} and N_{10}. The higher intensity of fluorescence emission of N_{10} is attributed to the smaller size of ZnO supported on the surface of zeolite.

Photo-oxidation degradation of nano-ZnO-supported 13X zeolite-filled PPR composites

Infrared spectrometry is a powerful tool to study photo-oxidation degradation of PP [15–17, 33]. Similarly, it can be used to study the photo-oxidation degradation of

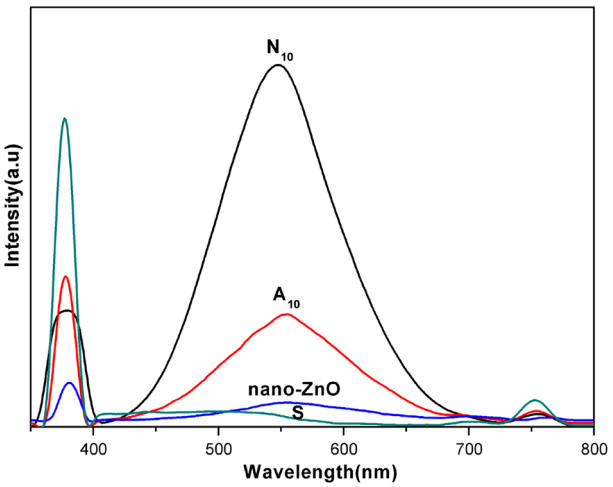

Fig. 3 Fluorescence spectra of 13X zeolie (S), nano-ZnO-supported 13X zeolite (A_{10} and N_{10}) and nano-ZnO at room temperature

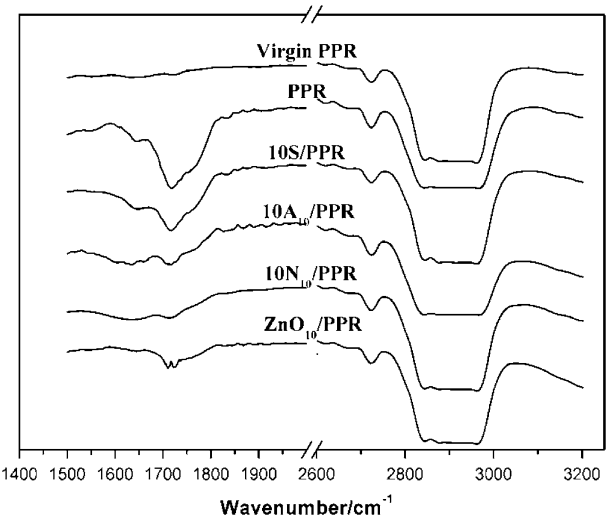

Fig. 4 FTIR spectra of 1,500–2,000 and 2,600–3,200 cm^{-1} for PPR, 10S/PPR, $10A_{10}$/PPR, $10N_{10}$/PPR and ZnO_{10}/PPR after UV irradiation for 120 h

PPR and its composites. Figure 4 is the infrared spectrum of PPR and its composites after UV irradiation for 120 h. It can be seen that the UV irradiation significantly increased the intensities of carbonyl band between 1,650 and 1,800 cm^{-1} for PPR, 10S/PPR and ZnO_{10}/PPR composites. However, no significant change was observed for the intensities of carbonyl band between 1,650 and 1,800 cm^{-1} in the $10A_{10}$/PPR and $10N_{10}$/PPR composites. This experimental result indicated that photo-oxidation degradation resistance of $10A_{10}$/PPR and $10N_{10}$/PPR composites was higher than that of ZnO_{10}/PPR containing the same content of ZnO. For quantitative analysis of the photo-oxidation degradation, the carbonyl index is calculated and its change with UV-irradiation time is shown in Fig. 5. It can be observed that the carbonyl index of PPR and its composites increased with increasing UV-irradiation time, especially 10S/PPR composites. While no significant change of carbonyl index was observed in the $10A_{10}$/PPR, $10N_{10}$/PPR and ZnO_{10}/PPR composites for UV irradiation for 90 h. This result demonstrated that the addition of 13X zeolite accelerated the photo-oxidation degradation of PPR. Nano-ZnO-supported 13X zeolite and nano-ZnO-filled PPR composites can increase the photo-oxidation degradation resistance of PPR. However, when PPR and its composites were UV irradiated for 120 h, the carbonyl index of nano-ZnO-filled PPR composites significantly increased and the carbonyl index of nano-ZnO-supported 13X zeolite-filled PPR composites had little change. It is indicated that the nano-ZnO-supported 13X zeolite-filled PPR composites has higher photo-oxidation degradation resistance than nano-ZnO-filled PPR composites.

To further study the effect of nano-ZnO-supported 13X zeolite, the photo-oxidation degradation of PPR composites filled with different contents of nano-ZnO-supported 13X zeolite (N_{10}) and nano-ZnO was investigated. It can be

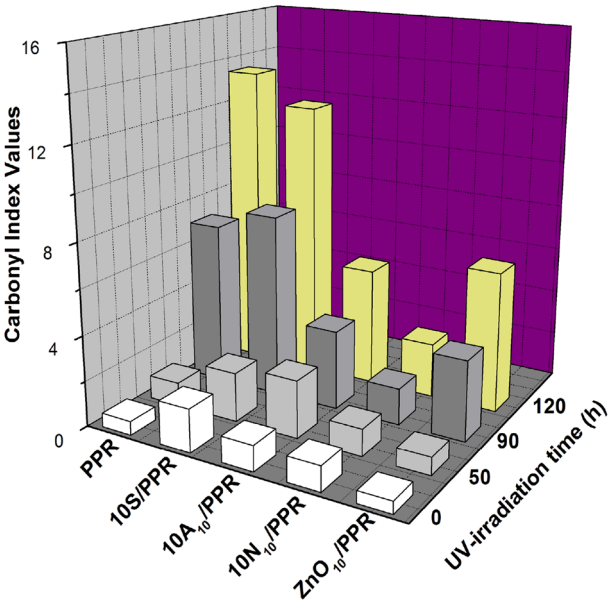

Fig. 5 Carbonyl index values as a function of UV-irradiation time for PPR and its composites

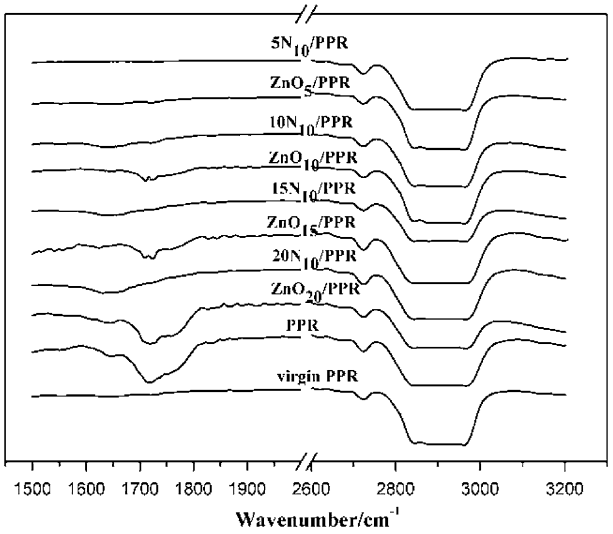

Fig. 6 FTIR spectra of 1,500–2,000 and 2,600–3,200 cm^{-1} for PPR and PPR composites filled with different contents of N_{10} or ZnO after UV irradiation for 120 h

observed from Figs. 6, 7 that the carbonyl band between 1,650 and 1,800 cm^{-1} and the carbonyl index increased with increase in the content of N_{10}. It is attributed to the two opposite effects of UV screening and photocatalysis of ZnO on film photo-

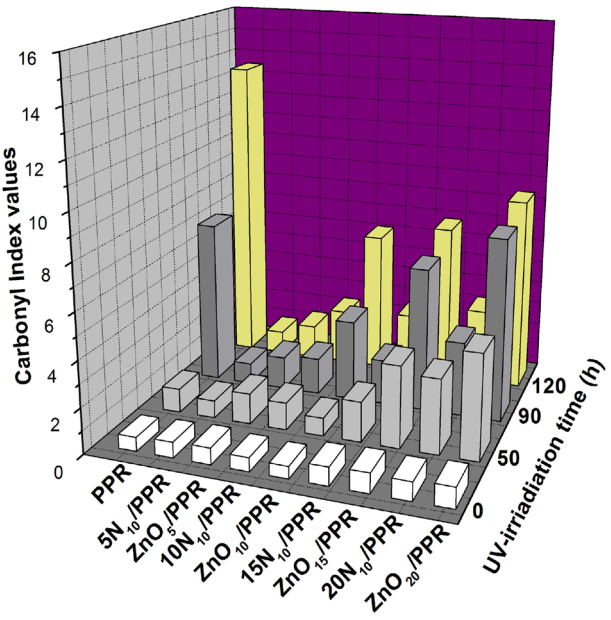

Fig. 7 Carbonyl index values as a function of UV-irradiation time for PPR and PPR composites filled with different contents of N_{10} or nano-ZnO

degradation [34, 35]. The carbonyl index of PPR composites filled with different contents of nano-ZnO-supported 13X zeolite is significantly lower than that of nano-ZnO-filled PPR composites. Therefore, it is considered that the photo-oxidation degradation resistance of nano-ZnO-supported 13X zeolite-filled PPR composites is better than nano-ZnO directly filled PPR composites.

Antimicrobial properties of nano-ZnO-supported 13X zeolite-filled PPR composites

The antimicrobial ability of nano-ZnO-supported 13X zeolite-filled PPR composites was evaluated quantitatively in fluid nutrient medium. The antimicrobial reduction rate, Y value, is listed in Table 2 for PPR and its composites to *S. aureus* and *E. coli*. It can be observed that pure PPR and 13X zeolite-filled PPR composite (5S/PPR) has no antibacterial ability. The nano-ZnO-supported 13X zeolite-filled PPR composites have antimicrobial properties and the antimicrobial ability of its filled PPR composites increases with increase in nano-ZnO-supported 13X zeolite content shown in Fig. 8. The Y values of $20A_{10}$/PPR are 100 % and 99.4 % to *E. coli* and *S. aureus*, respectively, and higher than those of PPR filled by nano-ZnO as the same content of ZnO as A_{10} filled PPR composites. This result indicated that the nano-ZnO-supported 13X zeolite-filled PPR composites have stronger antibacterial ability than nano-ZnO-filled PPR composites. It is suggested that the antibacterial ability of ZnO-filled PPR composites depends on the morphology

Table 2 The antibacterial reduction rate of PPR and its composites

Sample	*Escherichia coli*		*Staphylococcus aureus*	
	Abs	*Y* (%)	Abs	*Y* (%)
Blank	1.486	0	1.542	0
PPR	1.554	−4.6	1.754	−13.7
5S/PPR	1.722	−15.9	1.542	−15.0
$5A_{10}$/PPR	0.678	54.4	0.771	50.0
$10A_{10}$/PPR	0.618	58.4	0.648	58.0
$15A_{10}$/PPR	0.027	98.2	0.085	94.5
$20A_{10}$/PPR	0.000	100.0	0.010	99.4
$5N_{10}$/PPR	0.962	35.3	0.842	45.4
$10N_{10}$/PPR	0.531	64.3	0.456	70.4
$15N_{10}$/PPR	0.056	96.3	0.103	93.3
$20N_{10}$/PPR	0.023	98.5	0.069	95.5
ZnO_{20}/PPR	0.094	93.7	0.036	97.7

and surface area of ZnO as the antimicrobial agent. The nano-ZnO is generally dispersed into the PPR matrix in large agglomerate state resulting in lower surface area of ZnO, while ZnO with filamentous morphology supported on the surface of zeolite has higher specific surface area, leading to increase in the antibacterial ability of filled PPR composites.

Dispersion and morphology of nano-ZnO-supported 13X zeolite-filled PPR composites

To analyze the dispersion and morphology of ZnO in the PPR matrix, the fracture surface of 20S/PPR, $20A_{10}$/PPR, $20N_{10}$/PPR and ZnO_{20}/PPR composites fractured in fluid nitrogen was observed with SEM. Figure 9 shows the fracture surface morphology of neat zeolite, nano-ZnO-supported 13X zeolite and nano-ZnO-filled PPR composites. For the zeolite-filled PPR composites, it can be observed that although the zeolite is uniformly dispersed in the PPR matrix, there is no interface adhesion between the zeolite and PPR and the fracture mainly happened in the interface between zeolite and PPR. The zeolite particles are easy to peel off from the PPR matrix, resulting in the interface fracture. For the nano-ZnO-supported 13X zeolite-filled PPR composites, not only nano-ZnO-supported 13X zeolite particles were dispersed uniformly in filled PPR composites, but also there was also a strong interface adhesion between zeolite and PPR, resulting in the PPR matrix fracture. For the nano-ZnO-filled PPR composites, it is difficult to disperse the nano-ZnO in the PPR matrix uniformly due to easy aggregation. Therefore, the ZnO supported on the surface of zeolite not only is in favor of the dispersion of inorganic particles in the PPR matrix, but can also improve the interface adhesion between the zeolite particles and PPR matrix. Meanwhile, the ZnO supported on the surface of

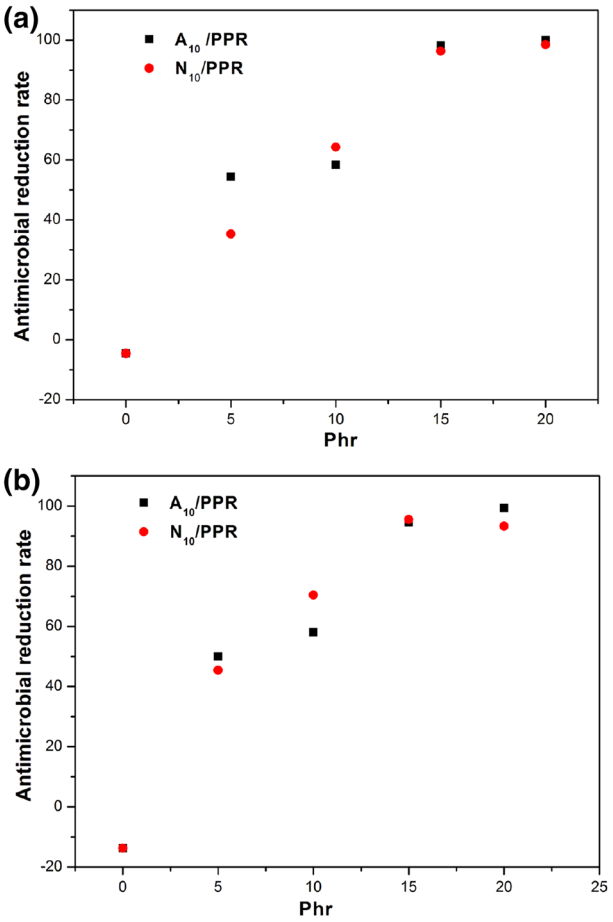

Fig. 8 Antibacterial reduction rate of A_{10}- and N_{10}-filled PPR composites toward *E. coli* (**a**) and *S. aureus* (**b**)

zeolite particles can endow higher photo-oxidation degradation resistance and antimicrobial ability for the PPR matrix.

Crystallization behavior and melting characteristics of nano-ZnO-supported 13X zeolite-filled PPR composites

Figure 10 presents the crystallization and melting behavior of PPR and filled PPR composites; the corresponding DSC data are listed in Table 3. It can be observed that addition of ZnO had no influence on the crystallization temperature of PPR. This suggested that ZnO has no heterogeneous nucleation for PPR crystallization [31]. Addition of 10 phr 13X zeolite increased the crystallization temperature of PPR from 102.4 to 107.3 °C, indicating the heterogeneous nucleation of 13X zeolite

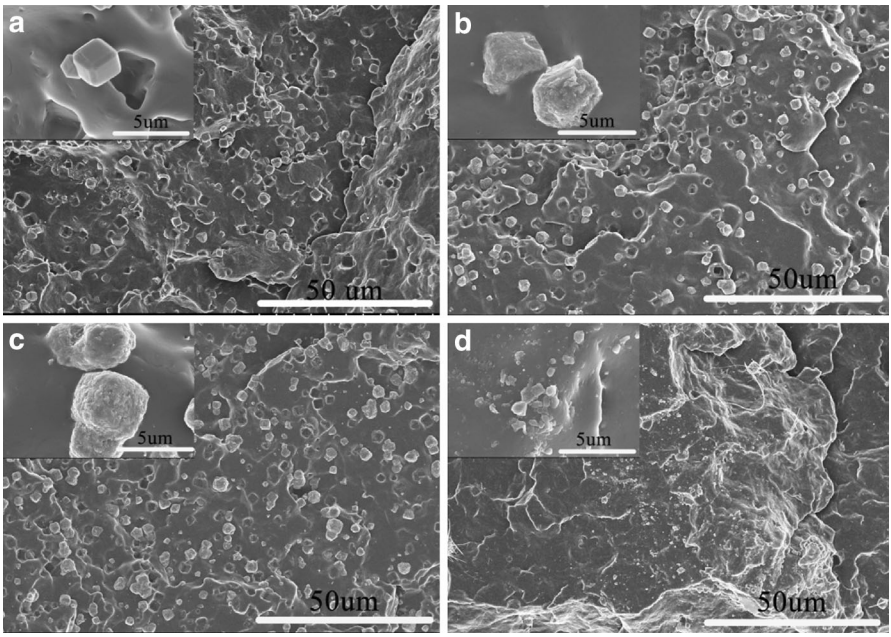

Fig. 9 SEM morphologies of 20S/PPR (**a**), $20A_{10}$/PPR (**b**), $20N_{10}$/PPR (**c**) and ZnO_{20}/PPR (**d**), respectively

for PPR crystallization. The crystallization temperature of 10 phr A_{10}- or N_{10}-filled PPR composites are 106.0 and 104.0 °C, respectively, which are lower than that of 10 phr 13X zeolite-filled PPR composites. The results indicated that the formation of ZnO on the surface of zeolite decreased the heterogeneous nucleation of zeolite for PPR crystallization. The crystallization temperature of ZnO-filled PPR composites is dependent on the morphology of ZnO [23]. The $10A_{10}$/PPR and $10N_{10}$/PPR composites with different crystallization temperatures are attributed to the different morphologies of ZnO on the surface of zeolite. However, 13X zeolite, nano-ZnO-supported 13X zeolite and nano-ZnO have no influence on the melting behavior and degree of crystallization of PPR composites.

Conclusions

To improve the functionality of ZnO, ZnO supported on the surface of 13X zeolite was prepared with $Zn(Ac)_2$ and $Zn(NO_3)_2$ aqueous solution and zeolite. The prepared nano-ZnO-supported 13X zeolite particles and their filled PPR composites exhibit better photo-oxidation degradation resistance and higher antimicrobial ability than nano-ZnO and its filled PPR composites for *S. aureus* and *E. coli*. The antimicrobial reduction rate increased with increasing nano-ZnO-supported 13X zeolite content. The interface adhesion between nano-ZnO-supported 13X zeolite

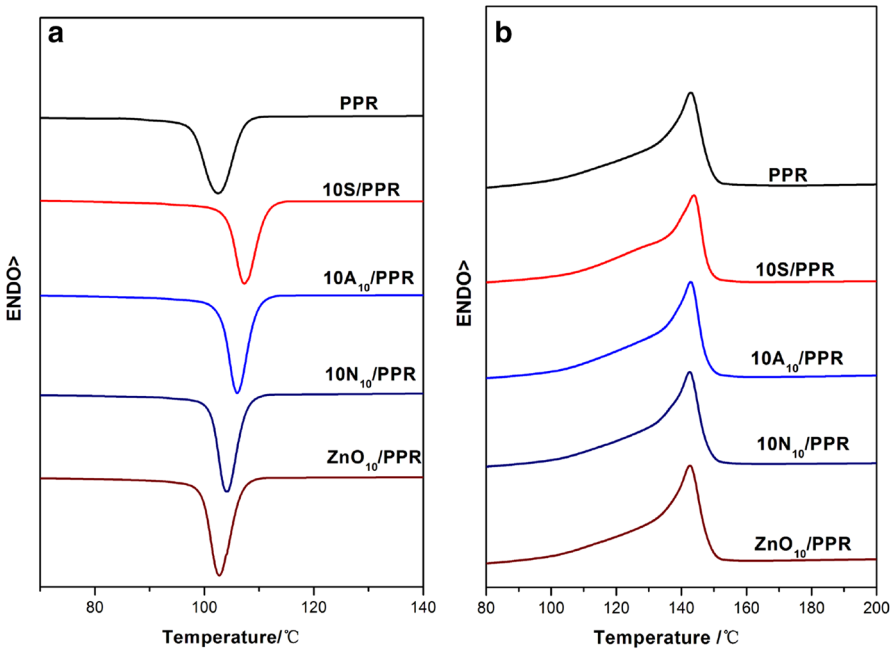

Fig. 10 DSC crystallization (**a**) and melting (**b**) curves with a heating and cooling rate of 10 °C/min for PPR and its composite

Table 3 DSC data of PPR and its composites

Sample	T_c (°C)	ΔH_c (J/g)	T_m (°C)	ΔH_m (J/g)	X_c (%)
PPR	102.4	61.6	143.0	56.8	27.2
10S/PPR	107.3	61.6	143.8	57.8	27.7
$10N_{10}$/PPR	104.0	63.5	142.6	60.7	29.0
$10A_{10}$/PPR	106.0	66.0	142.9	62.1	29.7
ZnO_{10}/PPR	102.8	64.9	142.5	60.2	28.8

and PPR matrix is stronger than that between 13X zeolite and PPR matrix. The heterogeneous nucleation of nano-ZnO-supported 13X zeolite increased the crystallization temperature of PPR, but had no influence on the melting behavior of PPR.

Acknowledgments The project was supported by the Natural Science Foundation of China (Grant No. 51173208, 51373202) and Natural Science Foundation of Guangdong (Grant No. S2011020001212). The authors wish to acknowledge Prof Ma Lin for supplying the devices for antibacterial experiments.

References

1. Jia F, Jia F (2013) Study of β-nucleated controlled-rheological polypropylene random copolymer: crystallization behavior and a possible degradation mechanism. Ind Eng Chem Res 52:761–770

2. Papageorgiou DG, Bikiaris DN, Chrissafis K (2012) Effect of crystalline structure of polypropylene random copolymers on mechanical properties and thermal degradation kinetics. Thermochim Acta 543:288–294
3. McNally T, McShane P, Nally G, Murphy W, Cook M, Miller A (2002) Reology, phase morphology, mechanical, impact and thermal properties of polypropylene/metallocene catalysed ethylene 1-octene copolymer blends. Polymer 43:3785–3793
4. Luo F, Zhu Y, Wang K, Deng H, Chen F, Zhang Q, Fu Q (2012) Enhancement of β-nucleated crystallization in polypropylene random copolymer via adding isotactic polypropylene. Polymer 53:4861–4870
5. Cao J, Lu Q (2011) Crystalline structure, morphology and mechanical properties of β-nucleated controlled-rheology polypropylene random copolymers. Polym Test 30:899–906
6. Luo F, Wang K, Wang JW, Deng H, Zhang Q, Chen F, Fu Q, Na B (2011) Tailoring toughness of injection molded bar of polypropylene random copolymer through processing melt temperature. Polym Int 60:1705–1714
7. Chen HB, Karger-Kocsisb J, Wu JS, Varga J (2002) Fracture toughness of α- and β-phase polypropylene homopolymers and random- and block-copolymers. Polymer 43:6505–6514
8. Hong JI, Winberg P, Schadler LS, Siegel RW (2005) Dielectric properties of zinc oxide/low density polyethylene nanocomposites. Mater Lett 59:473–476
9. Wang J, Liu P, Fu X, Li Z, Han W, Wang X (2009) Relationship between oxygen defects and the photocatalytic property of ZnO nanocrystals in nafion membranes. Langmuir 25:1218–1223
10. Dutta RK, Sharma PK, Bhargava R, Kumar N, Pandey AC (2010) Differential susceptibility of escherichia coli cells toward transition metal-doped and matrix-embedded ZnO nanoparticles. Phys Chem B 114:5594–5599
11. Tankhiwale R, Bajpai SK (2012) Preparation, characterization and antibacterial applications of ZnO-nanoparticles coated polyethylene films for food packaging. Colloids Surf B 90:16–20
12. Ma J, Liu J, Bao Y, Zhu Z, Wang X, Zhang J (2013) Synthesis of large-scale uniform mulberry-like ZnO particles with microwave hydrothermal method and its antibacterial property. Ceram Int 39:2803–2810
13. Zarrinkhameh M, Zendehnam A, Hosseini SM (2013) Electrochemical, morphological and antibacterial characterization of PVC based cation exchange membrane modified by zinc oxide nanoparticles. J Polym Res 20:283–291
14. Indolia AP, Gaur MS (2013) Optical properties of solution grown PVDF-ZnO nanocomposite thin films. J Polym Res 20:43–50
15. Zhao H, Li RKY (2006) A study on the photo-degradation of zinc oxide (ZnO) filled polypropylene nanocomposites. Polymer 47:3207–3217
16. Chandramouleeswaran S, Mhaske ST, Kathe AA, Varadarajan PV, Prasad V, Vigneshwaran N (2007) Functional behavior of polypropylene/ZnO-soluble starch nanocomposites. Nanotechnology 18:1–8
17. Salla J, Pandey KK, Srinivas K (2012) Improvement of UV resistance of wood surfaces by using ZnO nanoparticles. Polym Degrad Stab 97:592–596
18. Venkatesha TG, Arthoba Nayaka Y, Viswanatha R, Vidyasagar CC, Chethana BK (2012) Electrochemical synthesis and photocatalytic behavior of flower shaped ZnO microstructures. Powder Technol 225:232–238
19. Hassana NK, Hashima MR, Bououdina M (2013) One-dimensional ZnO nanostructure growth prepared by thermal evaporation on different substrates: ultraviolet emission as a function of size and dimensionality. Ceram Int 39:7439–7444
20. Abdolmalek A, Mallakpour S, Borandeh S (2012) Effect of silane-modified ZnO on morphology and properties of bionanocomposites based on poly(ester-amide) containing tyrosine linkages. Polym Bull 69:15–28
21. Khrenov V, Schwager F, Klapper M, Koch M, Müllen K (2007) Compatibilization of inorganic particles for polymeric nanocomposites. Optimization of the size and the compatibility of ZnO particles. Polym Bull 58:799–807
22. Ma XY, Zhang WD (2009) Effects of flower-like ZnO nanowhiskers on the mechanical, thermal and antibacterial properties of waterborne polyurethane. Polym Degrad Stab 94:1103–1109
23. Zheng A, Zheng Y, Guo Y, Qiu S, Cheng L (2012) Effect of tetra-needle-shaped zinc oxide whisker (T-ZnO_w) on mechanical properties and crystallization behavior of isotactic polypropylene. Mater Des 34:691–698

24. Lepot N, Van Bael MK, Van Den Rul H, D'Haen J, Peeters R, Franco D, Mullens J (2011) Influence of incorporation of ZnO nanoparticles and biaxial orientation on mechanical and oxygen barrier properties of polypropylene films for food packaging applications. J Appl Polym Sci 120:1616–1623
25. Omar MF, Akil HM, Ahmad ZA, Mahmud SM (2012) The effect of loading rates and particle geometry on compressive properties of polypropylene/zinc oxide nanocomposites: experimental and numerical prediction. Polym Compos 33:99–108
26. Wen B, Ji B (2012) Crystallization behaviors and mechanical performance of polypropylene/tetrapod-shaped zinc oxide whisker composites. J Appl Polym Sci 124:138–144
27. Majid M, Hassan ED, Davoud A, Saman M (2011) A study on the effect of nano-ZnO on rheological and dynamic mechanical properties of polypropylene: experiments and models. Compos B 42:2038–2046
28. Li M, Li G, Jiang J, Tao Y, Mai K (2013) Preparation, antimicrobial, crystallization and mechanical properties of nano-ZnO-supported zeolite filled polypropylene random copolymer composites. Compos Sci Technol 81:30–36
29. Obadal M, Cermák R, Raab M, Verney V, Commereuc S, Fraïsse F (2005) Structure evolution of α- and β-polypropylenes upon UV irradiation: a multiscale comparison. Polym Degrad Stab 88:532–539
30. Rabello MS, White JR (1997) The role of physical structure and morphology in the photodegradation behaviour of polypropylene. Polym Degrad Stab 56:55–73
31. Pline WA, Lacy GH, Stromberg V, Hatzios KK (2001) Antibacterial activity of the herbicide glufosinate on pseudomonas syringae pathovar glycinea. Pestic Biochem Physiol 71:48–55
32. Neto PO, Ferreira MA, Yokoya F (2004) Screening for yeast with antibacterial properties from an ethanol distillery. Bioresour Technol 92:1–6
33. Jiang J, Li G, Ding Q, Mai K (2012) Ultraviolet resistance and antimicrobial properties of ZnO-supported zeolite filled isotactic polypropylene composites. Polym Degrad Stab 97:833–838
34. Bussière PO, Peyroux J, Chadeyron G, Therias G (2013) Influence of functional nanoparticles on the photostability of polymer materials: recent progress and furtherapplications. Polym Degrad Stab 98:2411–2418
35. Therias S, Larchè JF, Bussière PO, Gardette JL, Murariu M, Dubois P (2012) Photochemical behavior of polylactide/ZnO nanocomposite films. Biomacromolecules 13:3283–3291